

Mixed-Integer Programming Using a Bosonic Quantum Computer

Farhad Khosravi,¹ Artur Scherer,² and Pooya Ronagh^{1,3,4,5,*}

¹*1QB Information Technologies (1QBit), Vancouver, BC, Canada*

²*1QBit, Waterloo, ON, Canada*

³*Institute for Quantum Computing, University of Waterloo, Waterloo, ON, Canada*

⁴*Department of Physics & Astronomy, University of Waterloo, Waterloo, ON, Canada*

⁵*Perimeter Institute for Theoretical Physics, Waterloo, ON, Canada*

(Dated: June 9, 2022)

We propose a scheme for solving mixed-integer programming problems in which the optimization problem is translated to a ground-state preparation problem on a set of bosonic quantum field modes (qumodes). We perform numerical demonstrations by simulating a circuit-based optical quantum computer with each individual qumode prepared in a Gaussian state. We simulate an adiabatic evolution from an initial mixing Hamiltonian, written in terms of the momentum operators of the qumodes, to a final Hamiltonian which is a polynomial of the position and boson number operators. In these demonstrations, we solve a variety of small non-convex optimization problems in integer programming, continuous non-convex optimization, and mixed-integer programming.

I. INTRODUCTION

Achieving a quantum advantage in solving mathematical optimization problems will tremendously broaden the range of applications of quantum computers. To this end, a great variety of approaches has been explored, from the experimental realization of quantum annealers [1] to the design of circuit model quantum algorithms for optimization [2–4]. Quantum annealers rely on the analog simulation of an adiabatic evolution process, which restricts the sizes of optimization problems they can solve in the limited time available before the system decoheres. Quantum circuit model algorithms for optimization typically offer an asymptotic, yet modest, quadratic speedup compared to the exponentially costly exhaustive search. This quantum speedup relies on quantum amplitude amplification and estimation techniques [5], and will likely require very large fault-tolerant quantum computers [6] to solve problems of a size practical for real-world applications. In addition, both approaches perform quantum algorithms on a register of qubits, which restricts the types of optimization problems they can solve, especially in the absence of dense couplings between the qubits.

In this paper, we use a set of bosonic quantum field modes (or “qumodes”¹) to encode a mixed-integer programming (MIP) problem. We translate integer and continuous variables to different observables of the bosonic system. Non-negative integer variables are represented by the eigenstates of the number operators $\hat{n} = \hat{a}^\dagger \hat{a}$ of the qumodes. Here, \hat{a}^\dagger and \hat{a} are, respectively, the bosonic creation and annihilation operators. In contrast,

continuous variables are encoded in the continuous spectrum of the quadrature operators $\hat{x} = \frac{1}{\sqrt{2}}(\hat{a} + \hat{a}^\dagger)$ or $\hat{p} = \frac{1}{i\sqrt{2}}(\hat{a} - \hat{a}^\dagger)$, that is, the canonically conjugate position and momentum observables of quantum harmonic oscillators, respectively.

Computation using bosonic systems has been explored in various ways to date. Continuous-variable quantum computation (CVQC) [7] pertains to performing unitary transformations according to Hamiltonians that are polynomials of quadrature operators. In contrast, in boson sampling [8–10], quantum information is encoded in the discrete spectrum of the boson number operators. Both computing tasks are of experimental and theoretical interest in the particular case of quantum computation using Gaussian states [11, 12]. In addition, advances in measurement-based, one-way universal quantum computation using CVQC [13] and the creation of cluster states in optical settings [14, 15] provide promising prospects for experimental CVQC.

Computational significance. A mathematical programming problem is an optimization problem in which an objective function is optimized with respect to a set of variables satisfying a set of constraints. In MIP, both the objective function and constraints are polynomials of integer and continuous variables. Mixed-integer linear programming pertains to problems in which the objective function and constraints are linear functions of the variables. This is enough to obtain natural models for typical combinatorial and discrete optimization problems [16], including famous NP-hard optimization problems in constraint satisfaction, graph and network optimization, and job scheduling [17]. Mixed-integer nonlinear programming problems extend this class to a boundless domain of real-world applications in science, engineering, operations research, management, health care, decision making, and system control [18, 19]. Despite this flexible modelling power, classical algorithms for solving nonlinear and mixed-integer optimization problems scale poorly with respect to problem size [20]. For instance, solving

* Corresponding author: pooya.ronagh@1qbit.com

¹ The term “qumode” is commonly used to refer to the quantum harmonic oscillator associated with each single mode of a bosonic quantum field. Unlike in the case of qubits, quantum information is encoded in the infinite-dimensional Fock space associated with each qumode.

non-convex quadratic optimization problems is itself extremely challenging, to the extent that even verifying local optimality of their feasible points is NP-hard [21].

In this paper, we recast an MIP problem as the problem of preparing the ground state of a quantum Hamiltonian in a multi-mode Fock space, and then investigate an adiabatic scheme for finding the ground state of the Hamiltonian. However, other state preparation protocols, such as variational quantum algorithms [22], may be envisaged. Indeed, Verdon et al. [23] implement a continuous-variable analogue to the quantum approximate optimization algorithm (QAOA) [24] by writing the problem Hamiltonian in terms of one quadrature operator and the mixing Hamiltonian in terms of the other. However, to the best of our knowledge, the use of Fock states to encode integer variables in the context of solving MIP problems, and the capability and computational significance of solving mixed-integer non-convex global optimization problems using CVQC, have not been previously explored.

Numerical demonstrations. In Section III, we investigate the optimization of integer linear programming (ILP) problems, and solve a small example instance of the NP-hard unbounded knapsack problem [25]. In Section IV, we use a quadratic binary formulation of the NP-hard MAXCLIQUE problem to show that our scheme works, without any substantial modifications, in the case of nonlinear integer programming (NLIP) problems. Then, in Section V, we use the connection between the MAXCLIQUE problem and continuous non-convex optimization, established by Motzkin and Straus [26], to explore global non-convex optimization via both continuous and integer implementations of the MAXCLIQUE problem. We solve the problem using only the quadrature operators in the case of the continuous formulation and only the number operators in the case of the integer formulation. Finally, in Section VI, we demonstrate the application of our method in solving MIP problems, using an example instance of a sparse optimization problem. Such cardinality-constrained optimization problems are also NP-hard [27] and of practical importance in compressed sensing, signal processing, and computational finance [28].

For these demonstrations, we simulate a circuit model optical device, where individual qumodes are prepared as Gaussian states. An adiabatic evolution process is executed beginning with Gaussian states, followed by homodyne or photon number resolving measurements of the output qumodes, with the goal of preparing a state that overlaps substantially with the ground state of a problem Hamiltonian.

Experimental considerations. In a gate-based optical device, qumodes can be prepared as Gaussian states, after which they are acted upon by single- or two-qumode quantum optical gates integrated in photonic or optical fibre waveguides [29–31]. While suffering from their own limitations, quantum optical devices have an advantage in that they can operate at room temperature and

are easier to scale compared to other implementations of quantum processors [32].

Current realizations of experiments that implement photon–photon interactions restrict the practical realization of our method to solving integer programming problems that are at most quadratic in terms of integer variables. The computation is carried out by a set of gates implementing functions of the photon number operator, including the rotation gate $\hat{R}(\phi) = \exp(i\phi\hat{n})$, the Kerr gate $\hat{K}(\alpha) = \exp(i\alpha\hat{n}^2)$, and the cross-Kerr gate $\hat{C}\hat{K}(\alpha) = \exp(i\alpha\hat{n}_1\hat{n}_2)$, the last of which acts on the Fock space of two qumodes [33]. Together with the quadratic phase gate $\hat{P}(\alpha) = \exp(i\alpha\hat{p}^2)$ and the position displacement gate $\hat{X}(x) = \exp(ix\hat{p})$, this gate set is sufficient for solving integer linear and quadratic programming problems. To solve MIP problems, we require combined unitary gates that are functions of \hat{n} and one of the quadrature operators; for example, $\hat{X}\hat{N}(\alpha) = \exp(i\alpha\hat{x}_1^2\hat{n}_2)$. While unitary operations that use such a combination of quadrature and photon number operators have not been realized, we believe that our results will provide the impetus for the experimental realization of such unitary operations. Toward the realization of a universal gate set for CVQC, Yanagimoto et al. [34] propose a promising deterministic implementation of the non-Gaussian cubic phase gate $\exp(i\alpha\hat{x}^3)$, an approach worth exploring for implementing the two-qumode higher-order combined gates we have introduced.

Implementing non-Gaussian gates at a high level of fidelity remains an experimental challenge. While on-chip Mach–Zehnder interferometers based on beam splitters and thermo-optic phase shifters are efficiently fabricated for high-fidelity performance [35–37], the viability of creating photon–photon interactions, such as in Kerr and cross-Kerr gates, through $\chi^{(3)}$ third-order optical nonlinearity, has been subject to skepticism due to various challenges hampering the performance of these gates [38–41]. However, ongoing research on photon–photon interactions points to the possibility generating phase shifts from single-photon pulses using other methods such as quantum dots [42], Rydberg blockades [43, 44], and four-wave mixing using atomic systems [45]. These experiments show the physical possibility of creating Kerr interactions through a variety of approaches. The results presented in this paper motivate experimental efforts toward the realization of quantum unitary operations that incorporate photon–photon interactions. Here, we rely on the assumption of the existence of a viable method of implementing high-fidelity Kerr and cross-Kerr interactions (regardless of the method of their realization), which are necessary to implement the quantum operations required for MIP using CVQC.

II. ADIABATIC GROUND-STATE PREPARATION

We study the probability distribution of states prepared via adiabatic quantum computation (AQC). The time-dependent Hamiltonian considered for AQC is

$$\hat{H}(\tau) = (1 - \tau)\hat{H}_M + \tau\hat{H}_P, \quad (1)$$

where $\tau = t/T$ is the normalized time and T is the total evolution time. The Hamiltonian \hat{H}_P represents the *problem* Hamiltonian whose ground states encode the solutions to the optimization problem of interest, and \hat{H}_M is called a *mixing* Hamiltonian and is required to have an easy-to-prepare ground state and not to commute with \hat{H}_P .

When \hat{H}_M and \hat{H}_P have discrete spectra, the evolution time T is in $\mathcal{O}(\delta^{-2})$, where δ is the smallest spectral gap of \hat{H}_P for all τ [46]. Therefore, implementing this evolution in a scalable way via analog computation can be challenging [47]. While for AQC involving Hamiltonians with continuous spectra the evolution time cannot be bounded in terms of a well-defined spectral gap, results similar to the conventional adiabatic theorem [48] suggest that the evolution in time T deviates from identity by $\mathcal{O}(1/T)$. However, the evolution can be discretized and implemented on a fault-tolerant circuit model quantum device. To this end, we use the common technique of Trotterization to approximate the adiabatic time evolution. The resulting circuit consists of iterative applications of unitary evolutions according to \hat{H}_M and \hat{H}_P ,

$$\hat{U} = e^{-ib_k\hat{H}_M}e^{-ic_k\hat{H}_P} \dots e^{-ib_1\hat{H}_M}e^{-ic_1\hat{H}_P}, \quad (2)$$

to an initial state $|\psi_0\rangle$ prepared in the ground state of \hat{H}_M . The overall number of Trotter steps, denoted by k , directly pertains to the circuit depth of the algorithm. The choice of the coefficients in the exponents depends on the function describing the schedule. For a linear schedule as given in Eq. (1), $b_j = (k - j + \frac{1}{2})\frac{T}{k^2}$ and $c_j = (j - \frac{1}{2})\frac{T}{k^2}$. Note that the sum of the coefficients of both the mixing and problem Hamiltonians is equal to T , and that their coefficients decrease and increase linearly with each Trotter step j , respectively. In our numerical simulations, we find that the continuous AQC algorithm and its discretized version yield very similar final results for all of the problems studied. For this reason, except in the case of the feasibility problem (see Section III), we present the results only for the continuous algorithm.

The mixing Hamiltonians used in our work are of the form

$$\hat{H}_M = \sum_{i=1}^N (\hat{p}_i^2 - 2p_{0i}\hat{p}_i), \quad (3)$$

which is equivalent to $\sum_{i=1}^N (\hat{p}_i - p_{0i})^2$ whose ground state is the momentum eigenstate $|p_0\rangle = |p_{01}\rangle \otimes \dots \otimes |p_{0N}\rangle$. Here, N is the number of qumodes. The quantum

state $|p_0\rangle$ is a negatively and infinitely squeezed coherent state along the momentum axis [49]. Although such states are not physically realizable, we can approximate them with the squeezed coherent states $|\alpha, -\mathbf{r}\rangle$, where $\alpha = (\alpha_1, \alpha_2, \dots, \alpha_N)$ and $\mathbf{r} = (r_1, r_2, \dots, r_N)$. In all our simulations, $\alpha_j = ip_{0j}/\sqrt{2\hbar}$ and $r_j = r$ for all j , where r is an experimentally feasible squeezing parameter, for example, taking values between 0.5 and 0.8. As the values of p_{0i} increase, these states overlap increasingly less with the vacuum state. This is important, as the vacuum state is an eigenstate of the number operator that is used to construct the problem Hamiltonian, and having a large overlap between the initial state and the eigenstates of the problem Hamiltonian will impair the adiabatic ground-state preparation.

In general, the initial state parameter p_0 affects the final quantum states obtained via the adiabatic scheme and can be treated as a hyperparameter that gives us direct access to a continuum of the initial mixing Hamiltonians and the associated ground states to use in our algorithm. For example, if \hat{H}_P has degenerate ground states, p_0 can be tuned to amplify the amplitude of each of those states or, alternatively, to create a uniform superposition of all of those states (see Section S2). The latter is known as *fair sampling*, which is equivalent to Gibbs sampling at the zero temperature limit and is therefore a desirable property in machine learning [50, 51]. In addition, for a generic problem Hamiltonian written in terms of \hat{n} and \hat{x} operators, the mixing Hamiltonian above satisfies the non-commutativity relation $[\hat{H}_P, \hat{H}_M] \neq 0$.

III. INTEGER LINEAR PROGRAMMING

Every ILP problem can be written in the *canonical* form

$$\begin{aligned} & \text{minimize} && -\mathbf{c}^T \mathbf{n} \\ & \text{subject to} && \mathbf{A}^T \mathbf{n} \leq \mathbf{b} \quad \text{and} \quad \mathbf{n} \geq 0, \end{aligned} \quad (4)$$

where \mathbf{n} is a column vector of N integer variables, \mathbf{c} is the matrix of coefficients describing the objective function, and the matrix \mathbf{A} and column vector \mathbf{b} specify a system of ℓ inequality constraints on the variables. As mentioned above, we use the boson number observable for each of the involved bosonic modes to represent the corresponding entries of \mathbf{n} . Hence, the condition $\mathbf{n} \geq 0$ and the integrality of these variables are automatically satisfied.

Each inequality $a_j^T \mathbf{n} \leq b_j$, for $1 \leq j \leq \ell$, can be rewritten as an equality constraint $a_j^T \mathbf{n} - b_j + \eta_j = 0$ via an auxiliary variable $\eta_j \geq 0$. This requires the addition of ℓ ancillary qumodes. Assuming \mathbf{A} and \mathbf{b} have fractional entries, we can multiply them by their lowest common denominator to turn all of their entries into integers. We then use the number operator of the j -th ancillary qumode to represent η_j . Alternatively, η_j can be considered a continuous variable represented by the

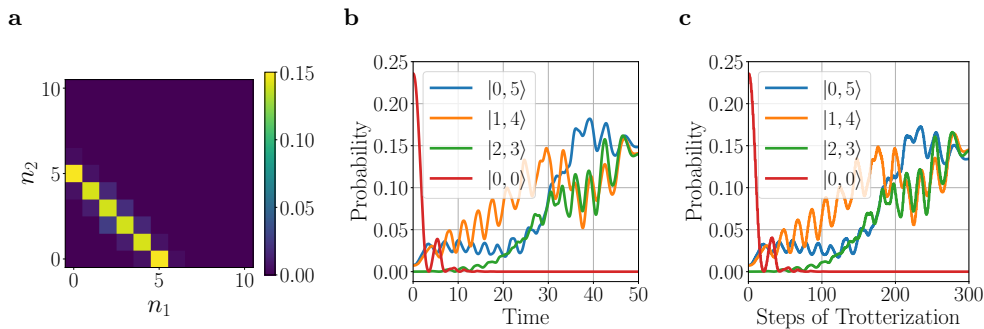


FIG. 1: Results for the feasibility problem specified by the equation $n_1 + n_2 = 5$, solved using AQC and its discretized form. (a) The probability distribution of the final quantum states in the two-qumode Fock basis $\{|n_1, n_2\rangle\}$. (b) The evolution of the probabilities of the dominant Fock states (in this case those that have the highest final probability amplitudes) during AQC for the total evolution time $T = 50$. (c) The evolution of the probabilities of the dominant Fock states during the execution of discretized AQC for a total number of Trotter steps $k = 300$. (b) and (c) The qumodes are initialized as the squeezed coherent states $|\alpha, -r\rangle$, where $\alpha = (\alpha_1, \alpha_2)$, with $\alpha_1 = \alpha_2 = 0.72i/\sqrt{2}$ and $r = 0.8$. Due to the symmetry between n_1 and n_2 , if the Fock state $|n_1, n_2\rangle$ is a solution, then $|n_2, n_1\rangle$ is also a solution. For this reason, only three of the six degenerate ground states are shown.

non-negative-valued observable x_j^2 of the j -th qumode. This, however, turns problem (4) into an MIP similar to those in Section VI.

To solve problem (4), we seek the ground state of the Hamiltonian

$$\hat{H}_P = - \sum_{i=1}^N c_i \hat{n}_i + \lambda \sum_{j=1}^{\ell} \left[\left(\sum_{i=1}^N A_{ij} \hat{n}_i \right) + \hat{\eta}_j - b_j \right]^2, \quad (5)$$

that is, by replacing the vectors \mathbf{n} and $\boldsymbol{\eta}$ with vectors of the photon number operators $\hat{\mathbf{n}}$ and $\hat{\boldsymbol{\eta}}$. Here, $\lambda > 0$ is a penalty coefficient tuned to suppress the infeasible subspace of the Hilbert space. We note that simulating the problem Hamiltonian (5) requires the implementation of unitary evolutions of the form $\exp(i\alpha\hat{n}_i\hat{n}_j)$, $\exp(i\alpha\hat{n}_i^2)$, and $\exp(i\alpha\hat{n}_i)$, which can all be achieved using cross-Kerr, Kerr, and rotation operations, respectively.

As a first example in our study of ILP problems, we consider the simple problem of solving the equation $n_1 + n_2 = 5$ over the integer domain. This simple equation can be re-written in the canonical form (4) by setting

$$A = \begin{pmatrix} 1 & -1 \\ 1 & -1 \end{pmatrix}, \quad \mathbf{b} = \begin{pmatrix} 5 \\ -5 \end{pmatrix}, \quad \text{and} \quad c = \begin{pmatrix} 0 \\ 0 \end{pmatrix},$$

that is, by imposing two inequalities, $n_1 + n_2 \leq 5$ and $-n_1 - n_2 \leq -5$, to determine the feasible domain. As such a problem does not effectively minimize an objective function but requires the finding of integer solutions only to a set of constraints, it is known as a *feasibility problem*. For this reason, we avoid reformulating the problem in the canonical form (as it would require employing four qumodes) and instead find the ground states of $\hat{H}_P = (\hat{n}_1 + \hat{n}_2 - 5)^2$.

Figure 1a shows the probability distribution of the results of measuring the final state in the two-mode Fock basis prepared using AQC. The probability amplitudes of the quantum states evolved over time via AQC and through its discretized form are depicted

in Figs. 1b and 1c, respectively. The two methods yield similar results, with the most-likely measurement outcomes corresponding to the six degenerate Fock states $|0, 5\rangle, |1, 4\rangle, |2, 3\rangle, |3, 2\rangle, |4, 1\rangle$, and $|5, 0\rangle$ representing the solutions of the ILP problem. We observe that the ground-state amplitudes are amplified by the adiabatic scheme while those of the other Fock states are suppressed. We tune p_{0i} in the mixing Hamiltonian (3) to achieve fair sampling (see Section S2).

We now consider a more interesting ILP problem in the canonical form. In the *knapsack problem*, a set of items and a knapsack are considered, where each item i has a value v_i and a weight w_i associated to it, and the knapsack has a total capacity W . The goal is to insert a number of items into the knapsack such that their selection maximizes the sum of the values of items in the knapsack while not exceeding its capacity. In typical logistics scenarios, however, each item is of a *type* i and we are allowed to choose any number of items of that type. This is called the *unbounded knapsack problem* (UKP), which can be formulated in the canonical form (4) as follows:

$$\begin{aligned} & \text{minimize} && - \sum_{i=1}^N v_i n_i \\ & \text{subject to} && \sum_{i=1}^N w_i n_i \leq W, \quad n_i \geq 0 \text{ for all } i. \end{aligned} \quad (6)$$

The integer variables n_i determine how many of each item type, if any, can be included in the knapsack.

Figure 2 shows the time progress of AQC for solving the UKP instance

$$\begin{aligned} & \text{minimize} && - n_1 - 2n_2 \\ & \text{subject to} && 4n_1 + 1.5n_2 \leq 11, \quad n_1, n_2 \geq 0, \end{aligned} \quad (7)$$

which has a unique optimal solution $(n_1, n_2) = (0, 7)$. We observe that the state $|\psi\rangle = |0, 7\rangle$ is amplified by AQC while all other Fock states are suppressed.

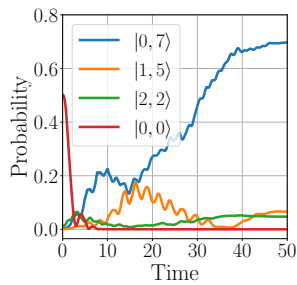


FIG. 2: State evolution during the execution of continuous AQC to solve the unbounded knapsack problem instance (7) using the total evolution time $T = 50$. The initial states are the squeezed coherent states $|\alpha, -r\rangle$, where $\alpha = (\alpha_1, \alpha_2, \alpha_3)$, with $\alpha_1 = \alpha_2 = \alpha_3 = \frac{0.25i}{\sqrt{2}}$ and $r = 0.8$. Note that the third state corresponds to the ancillary qumode, which is traced over in calculating the probabilities at the end of AQC. The penalty coefficient used is $\lambda = 4$.

IV. NONLINEAR INTEGER PROGRAMMING

In NLIP problems, both the objective functions and the constraints can be nonlinear functions of the integer variables. Such problems can be converted into ILP problem instances; however, this is at the cost of requiring additional qumodes. In this section, we show that NLIP problems can be solved directly on a bosonic quantum computer.

We use the MAXCLIQUE problem [52] as our working example. In this section, we consider a binary NLIP formulation of this problem, and in Section V we solve an integer NLIP formulation as well as a non-convex continuous formulation. In the MAXCLIQUE problem, a graph $G = (V, E)$ is given, where V is the set of vertices of G and E is the set of edges. Each edge $e \in E$ is a pair of vertices $\{i, j\} \subseteq V$. The set of edges can be represented by a symmetric adjacency matrix A , wherein $A_{ij} = 1$ if $\{i, j\}$ is in E , and $A_{ij} = 0$ otherwise. The goal of the MAXCLIQUE problem is to find the largest *complete* subgraph of G , that is, to find the largest subset $S \subseteq V$ such that all pairs of vertices in S are connected by an edge. In what follows, we also use S to denote the subgraph it determines (see Fig. 3a for an example).

Let $n_i \in \{0, 1\}$ represent the selection of vertex i in the maximum clique. Then, the following NLIP formulation can be used to solve the MAXCLIQUE problem:

$$\begin{aligned} & \text{minimize} && - \sum_i n_i \\ & \text{subject to} && \mathbf{n}^T (\mathbf{1} - A) \mathbf{n} = 0, \\ & && n_i \in \{0, 1\} \text{ for all } i. \end{aligned} \quad (8)$$

Here, $\mathbf{1}$ is the $N \times N$ matrix with every element equal to 1. We thus write the following problem Hamiltonian in terms of the number operators of the qumodes:

$$\hat{H}_P = - \sum_i \hat{n}_i + \lambda \sum_{i,j} (1 - A_{ij}) \hat{n}_i \hat{n}_j + \mu \sum_i \hat{n}_i (\hat{n}_i - 1). \quad (9)$$

The first term corresponds to the objective function of problem (8) and the second term penalizes any violation

of the adjacency constraint of problem (8). The last term restricts our search to the subspace of the Fock space corresponding to the eigenvalues 0 or 1 for the number operators of the qumodes. It is easy to see that any values of $\lambda > \frac{1}{2}$ and $\mu > 1$ suffice.

We apply AQC to the MAXCLIQUE problem for the graph shown in Fig. 3a. In Fig. 3b, we plot the three largest probabilities at the end of the adiabatic evolution. The two degenerate states representing the maximum cliques correspond to the vertices $\{1, 2, 4\}$ and $\{1, 3, 4\}$. Thus, in Fig. 3b, the probability amplitudes of the five-mode Fock states $|1, 1, 0, 1, 0\rangle$ and $|1, 0, 1, 1, 0\rangle$ converge to large values.

V. NON-CONVEX GLOBAL OPTIMIZATION

Non-convex continuous functions are difficult to optimize classically even when they contain no discrete variables [20]. For instance, Motzkin and Straus [26] provide a continuous formulation of the NP-hard MAXCLIQUE problem. As in the previous section, we let A denote the adjacency matrix of a graph G . Then, according to the Motzkin–Straus theorem, the optimal solutions of the continuous quadratic programming problem,

$$\begin{aligned} & \text{minimize} && -x^T A x \\ & \text{subject to} && \sum_i x_i = 1, \quad x_i \geq 0 \text{ for all } i, \end{aligned} \quad (10)$$

have nonzero entries $x_i = \frac{1}{\xi}$ for $i \in S$, where S is a maximum clique of G , and $x_i = 0$ for all $i \notin S$. Here, $\xi = |S|$ is the size of the one or possibly many maximum cliques.

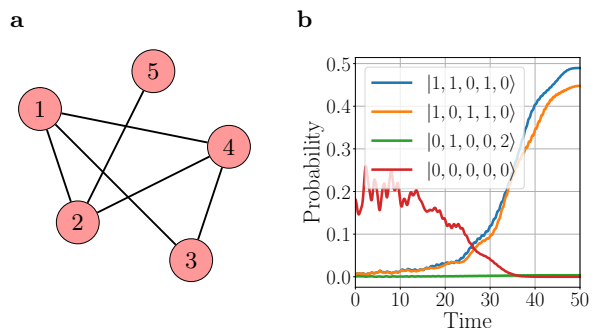


FIG. 3: (a) Example graph with five vertices, used as a MAXCLIQUE problem instance in our analysis. The graph contains two maximum cliques that are the subgraphs determined by the vertices $\{1, 2, 4\}$ and $\{1, 3, 4\}$. (b) State evolution during AQC to solve the MAXCLIQUE problem instance. We use the problem Hamiltonian (8) with $\lambda = 1$ and $\mu = 6$, and simulate the evolution of five qumodes all initialized as the squeezed coherent states $|\alpha, -r\rangle$, where $\alpha = (\alpha_1, \alpha_2, \dots, \alpha_5)$, with $\alpha_j = 0.55i/\sqrt{2}$ for all j and $r = 0.5$, for a total evolution time of $T = 50$. The degenerate ground states are $|1, 1, 0, 1, 0\rangle$ and $|1, 0, 1, 1, 0\rangle$. The next largest probability amplitude (green curve) observed has two photons in the fifth qumode. However, this state is not a ground state of Hamiltonian (8). The probability of the vacuum state $|0, 0, 0, 0, 0\rangle$ is shown using a red curve.

We use the position observable of the qumodes to represent continuous variables, and to impose the non-negativity of each x_i we substitute \hat{x}_i with \hat{x}_i^2 . The resulting problem Hamiltonian is

$$\hat{H}_P = - \sum_{i,j} A_{ij} \hat{x}_i^2 \hat{x}_j^2 + \lambda \left(\sum_i \hat{x}_i^2 - 1 \right)^2. \quad (11)$$

As all entries in the optimal solutions of problem (10) are 0 or $1/\xi$, we may substitute each x_i with n_i/ξ for an integer variable n_i and instead solve the problem

$$\begin{aligned} & \text{minimize} && -n^T A n \\ & \text{subject to} && \sum_i n_i = \sigma, \quad n_i \in \mathbb{Z}_{\geq 0} \text{ for all } i, \end{aligned} \quad (12)$$

using $\sigma = \xi$. However, ξ is not a priori known, but we may perform a binary search for its value using $\mathcal{O}(\log(|V|))$ choices of $\sigma \in \{1, \dots, |V|\}$, where $|V|$ is the number of vertices of the graph. In addition, we can infer the maximum cliques correctly even when $\sigma \geq \xi$ (see Section S3 for more detail). Using an approach similar to that of Section IV, the resulting problem Hamiltonian for this NLIP can be written as

$$\hat{H}_P = - \sum_{i,j} A_{ij} \hat{n}_i \hat{n}_j + \lambda \left(\sum_i \hat{n}_i - \sigma \right)^2. \quad (13)$$

We note that the Hamiltonians (9), (11), and (13) are all quartic in a and a^\dagger because \hat{n} and \hat{x}^2 are both quadratic in a and a^\dagger .

In Fig. 4a, we show the progression of AQC using the problem Hamiltonian (11) for solving the MAXCLIQUE problem for the graph in Fig. 3a. The solutions are found by performing a homodyne measurement of the \hat{x} observable for each mode, respectively (i.e., by projection on the $|x\rangle$ eigenstates). Here, $|1\rangle_x$ denotes a state with a measured value that is greater than or equal to $1/\sqrt{2|V|}$ for the eigenvalue of \hat{x} , while $|0\rangle_x$ denotes a state with a measured value less than $1/\sqrt{2|V|}$. The probabilities are found by performing measurements 1000 times. The five qumodes are measured consecutively with conditional homodyne measurements, and a histogram of the states $|n_1, n_2, n_3, n_4, n_5\rangle_x$ is generated, where $n_i \in \{0, 1\}$ according to the above definition. The probabilities are found from this histogram.

In Fig. 4b, we show the evolution of the probabilities of both the dominant quantum states (in this case those that have the highest final probability amplitudes) and the vacuum state, after performing AQC using the NLIP representation of the problem Hamiltonian (13). We observe that the continuous evolution shown in Fig. 4a is less performant (with a total success probability of observing a maximum clique of about 55%) than the probabilities shown in Fig. 3b and Fig. 4b for the integer formulations of the MAXCLIQUE problem (both with success probabilities greater than 90%). One reason for this

is the penalty relaxation in the Hamiltonian (11) is not equivalent to the original problem (10) and instead provides a lower bound for the optimal value of problem (10). Another reason is that, in our numerical simulations, the Fock space has been truncated to five dimensions due to limitations in classical computational resources. These two facts point to there being a broader probability distribution in the x direction of the phase space, which can cause a greater variance in the \hat{x} measurements.

We also observe a greater number of oscillations over time in the ground-state amplitudes for problem (12) compared to the binary formulation (8). This can be understood by the fact that Hamiltonian (13) has larger eigenvalues than Hamiltonian (9); the evolution via Hamiltonian (13) is populated by higher-number Fock states, whereas in Hamiltonian (9) only the values 0 or 1 are allowed for the boson number observable of each qumode. The amplitude oscillations can therefore be reduced by scaling down the problem Hamiltonian by a factor that is less than one while leaving the mixing Hamiltonian unaffected. Experimentally, performing such a normalization can be helpful in situations where the parameters of the quantum optical gates must remain within specific operating ranges. Finally, we note that the difference between the probabilities of observing the different degenerate ground states in Fig. 3b and Fig. 4b can be reduced by tuning the parameters of the initial states and the mixing Hamiltonian in order to achieve more “fair” samples. See Section S2 for more detail.

VI. MIXED-INTEGER PROGRAMMING

Finally, we demonstrate the application of our method in solving MIP problems (i.e., problems that consist of both integer and continuous variables). We use sparse

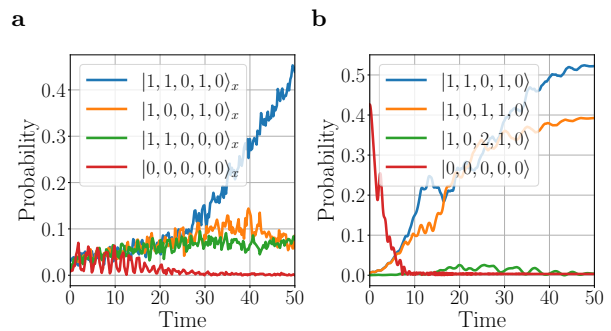


FIG. 4: Probability evolution in solving the MaxClique problem using the Motzkin–Straus framework, for the graph shown in Fig. 3a. (a) Solving the non-convex continuous quadratic problem (10) using the problem Hamiltonian (11). (b) Solving the non-convex integer quadratic problem (12) using the problem Hamiltonian (13). In both (a) and (b), the five qumodes are initialized as the squeezed coherent states $|\alpha, -r\rangle$, where $\alpha = (\alpha_1, \alpha_2, \dots, \alpha_5)$, with $\alpha_j = 0.55i/\sqrt{2}$ for all j and $r = 0.5$, and evolved using AQC for a total evolution time of $T = 50$. In both formulations, $p_0 = 0.55\hbar$ in the mixing Hamiltonian. The penalty coefficient is $\lambda = 2$ for the continuous formulation and $\lambda = 6$ for the integer formulation.

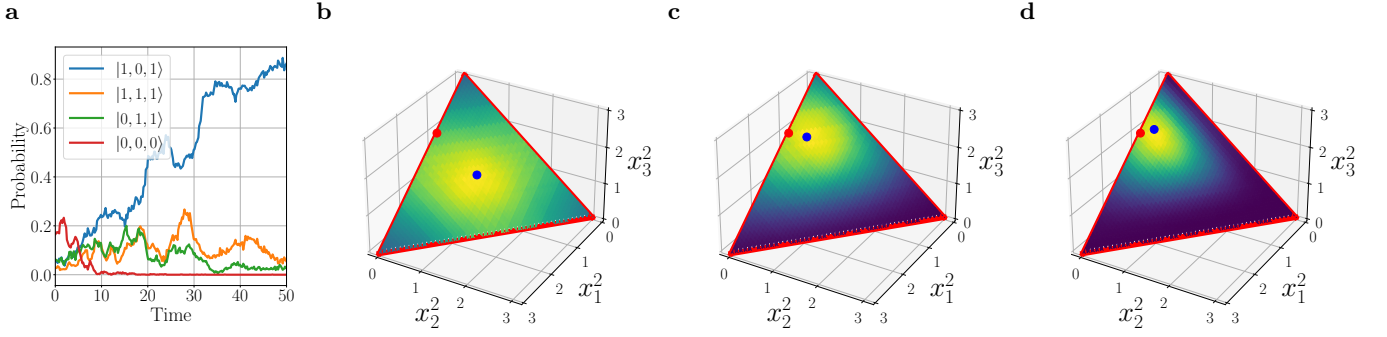


FIG. 5: Progression of AQC in finding the ground states of the problem Hamiltonian (16) representing the MIP problem (15). We use $(\lambda_1, \lambda_2, \lambda_3) = (1.2, 0.3, 0.3)$ and a total evolution time of $T = 50$. All initial coherent states have the squeezing parameter $r = -0.8$, and $p_0 = 0.55\hbar$, for all of the qumodes. (a) Time evolution of the probabilities of the states $|n_4, n_5, n_6\rangle$ that have the highest probabilities at the end of the adiabatic evolution, traced over the first three qumodes. The average measured values of the observables \hat{x}_i^2 for the first three qumodes, conditional upon the most probable quantum state $|n_4, n_5, n_6\rangle = |1, 0, 1\rangle$, at the end of AQC are $(\langle \hat{x}_1^2 \rangle, \langle \hat{x}_2^2 \rangle, \langle \hat{x}_3^2 \rangle) \simeq (0.7, 0.4, 1.6)$. The values of $\langle \hat{x}_i^2 \rangle$ for these qumodes are calculated by averaging 1000 homodyne measurements. (b)–(d) The time evolution of the probability distribution of the first three qumodes representing the continuous variables of the sparse optimization problem. The panels show the instantaneous probability distribution at (b) $t = 0$, (c) $t = T/2$, and (d) $t = T$, on the simplex. The discrepancy between the optimal solution (shown using a red dot) and the maximum of the probability distribution (blue dot) at $t = T$ is due to the truncation of the Fock space. Note that the variance of the distribution decreases throughout the adiabatic evolution.

optimization as our example.

Consider the problem

$$\begin{aligned} & \text{minimize} && f(x) = \sum_{i=1}^3 (x_i - \mu_i)^2 \\ & \text{subject to} && \sum_{i=1}^3 x_i = 3, \quad \|x\|_0 \leq 2, \\ & && x_i \geq 0 \text{ for all } i. \end{aligned} \quad (14)$$

Here, μ_i are constants. The objective function is a quadratic (convex) function of three continuous variables defined on the (also convex) positive two-dimensional simplex $S = \{(x_1, x_2, x_3) : \sum_{i=1}^3 x_i = 3\}$ in three dimensions. However, the feasible domain for the problem is the 2-skeleton of S consisting of those points in S that have at most two nonzero components, $S \cap \{x : \|x\|_0 \leq 2\}$. As a result, the constraints impose a non-convex feasible domain on the problem. Non-convex optimization problems as such are of practical significance in regression, machine learning, and signal processing [28].

We reformulate problem (14) as an MIP problem by adding the binary decision variables b_i :

$$\begin{aligned} & \text{minimize} && f(x) = \sum_{i=1}^3 (x_i b_i - \mu_i)^2 \\ & \text{subject to} && \sum_{i=1}^3 x_i b_i = 3, \quad \sum_{i=1}^3 b_i = 2, \\ & && b_i \in \{0, 1\} \text{ and } x_i \geq 0 \text{ for all } i. \end{aligned} \quad (15)$$

The assignment $b_i = 1$ indicates that the corresponding continuous variable x_i is allowed to attain nonzero values. To solve this MIP problem using our method, we use six qumodes with the operators \hat{x}_i^2 , for $i = 1, 2, 3$, on the first three qumodes representing the continuous variables, and

the number operators \hat{n}_i , for $i = 4, 5, 6$, representing the binary variables b_{i-3} . The MIP problem Hamiltonian is given by

$$\begin{aligned} \hat{H}_P = & \sum_{i=1}^3 (\hat{x}_i^2 \hat{n}_{i+3} - \mu_i)^2 + \lambda_1 \left(\sum_{i=1}^3 \hat{x}_i^2 \hat{n}_{i+3} - 3 \right)^2 \\ & + \lambda_2 \left(\sum_{i=1}^3 \hat{n}_{i+3} - 2 \right)^2 + \lambda_3 \sum_{i=1}^3 \hat{n}_{i+3} (\hat{n}_{i+3} - 1). \end{aligned} \quad (16)$$

Performing a homodyne measurement on the first three qumodes of the ground state of this Hamiltonian returns the solutions x_i , while a photon number resolving measurement on the second three qumodes reveals the nonzero support of the solution; that is, x_i is taken to be zero if n_{i+3} is zero.

Figure 5 shows the progression of AQC in finding the ground states of the problem Hamiltonian (16) representing the MIP problem (15). Figure 5a shows the time evolution of the quantum states $|n_4, n_5, n_6\rangle$ when traced over the first three qumodes. We use the constants $(\mu_1, \mu_2, \mu_3) = (1.0, 0.3, 2.0)$ in problem (14) for our example problem instance, yielding the optimal solution $(1.0, 0.0, 2.0)$. The quantum state $|n_4, n_5, n_6\rangle$ with the highest probability at the end of the adiabatic evolution is $|1, 0, 1\rangle$, which implies that x_2 should be taken to equal zero. Together with the measured values of the position operators for the first three qumodes, we infer that the solution is $(x_1, x_2, x_3) \simeq (0.7, 0.0, 1.6)$ for the MIP problem instance. The discrepancy with the optimal solution is due to the truncation of the Fock space to five dimensions. We have also verified that increasing the Fock space truncation from four to five dimensions reduces this discrepancy. Finally, Fig. 5b through Fig. 5d show the time evolution of the probability distribution of the \hat{x}_i^2 observables of the first three qumodes on the simplex.

VII. CONCLUSION

We have proposed a method for solving mixed-integer programming (MIP) problems using a set of programmable bosonic quantum field modes. Our approach takes advantage of the fact that the eigenspectrum of the bosonic number operators $\hat{n} = \hat{a}^\dagger \hat{a}$ consists of non-negative integers; thus, they can naturally represent integer variables. On the other hand, the quadrature operators $\hat{x} = \frac{1}{\sqrt{2}} (\hat{a} + \hat{a}^\dagger)$ and $\hat{p} = \frac{1}{i\sqrt{2}} (\hat{a} - \hat{a}^\dagger)$ have continuous spectra and do not commute with each other or with the number operator. Therefore, the MIP problem reduces to the problem of preparing the ground state of a Hamiltonian written in terms of \hat{n} and one of the quadrature operators. For instance, an adiabatic ground-state preparation scheme can be envisaged that uses a mixing Hamiltonian written in terms of the canonically conjugate quadrature operator of the one used in the Hamiltonian specifying the problem.

We have discussed the experimental realization and numerical simulation of this scheme on a continuous-variable, circuit model based quantum optical computer capable of preparing coherent Gaussian states, and performing rotation gates, Kerr gates, and cross-Kerr gates on them. At the end of the ground-state preparation scheme, homodyne and photon number resolving measurements were performed to return the optimal solutions to an MIP problem. We further analyzed a variety of linear and nonlinear MIP problems and provided numerical demonstrations on small instances of NP-hard optimization problems, specifically, the unbounded knapsack problem, the MAXCLIQUE problem, and cardinality-constrained optimization.

This work demonstrates that bosonic continuous-variable quantum computation devices can provide the natural processing capabilities required to solve MIP problems efficiently. Our results, moreover, motivate the experimental realization of a variety of non-Gaussian unitary gates on quantum optical platforms. In addition, our work illuminates an interesting direction for future theoretical research in investigating the computational complexity of the scheme proposed herein in view of adiabatic theorems for Hamiltonians with continuous spectra (similar to [48]).

ACKNOWLEDGEMENT

The authors thank our editor, Marko Bucyk, for his careful review and editing of the manuscript. The authors acknowledge the financial support received through the NSF's CIM Expeditions award (CCF-1918549). P. R. acknowledges the financial support of Mike and Ophelia Lazaridis, and Innovation, Science and Economic Development Canada.

Supplementary Information: Mixed-Integer Programming Using a Bosonic Quantum Computer

S1. ADIABATICITY

One common metric in studying the performance of the adiabatic quantum computation (AQC) algorithm is the *adiabaticity* of the method. This is done by studying the performance of the algorithm with respect to different total evolution time values T . Figure S1 shows the evolution of the success probabilities of solving the problem, as well as the probabilities of finding suboptimal solutions, for the integer and mixed-integer programming (MIP) problems discussed in the main manuscript. As expected, the solutions for all of the problems show the similar trend of starting at low success probabilities for a small total evolution time T , and plateauing to their final success probability values for larger values of T . These results indicate the optimum total evolution time for a given problem.

S2. FAIR SAMPLING

In this section, we look at fair sampling of the degenerate ground states of the integer programming problems studied. In many applications, it is undesirable that the optimizer gives preference to one or a few of the solutions [53] instead sampling all optimal solutions uniformly. For instance, in the example graph instance shown in Fig. 3a, fair

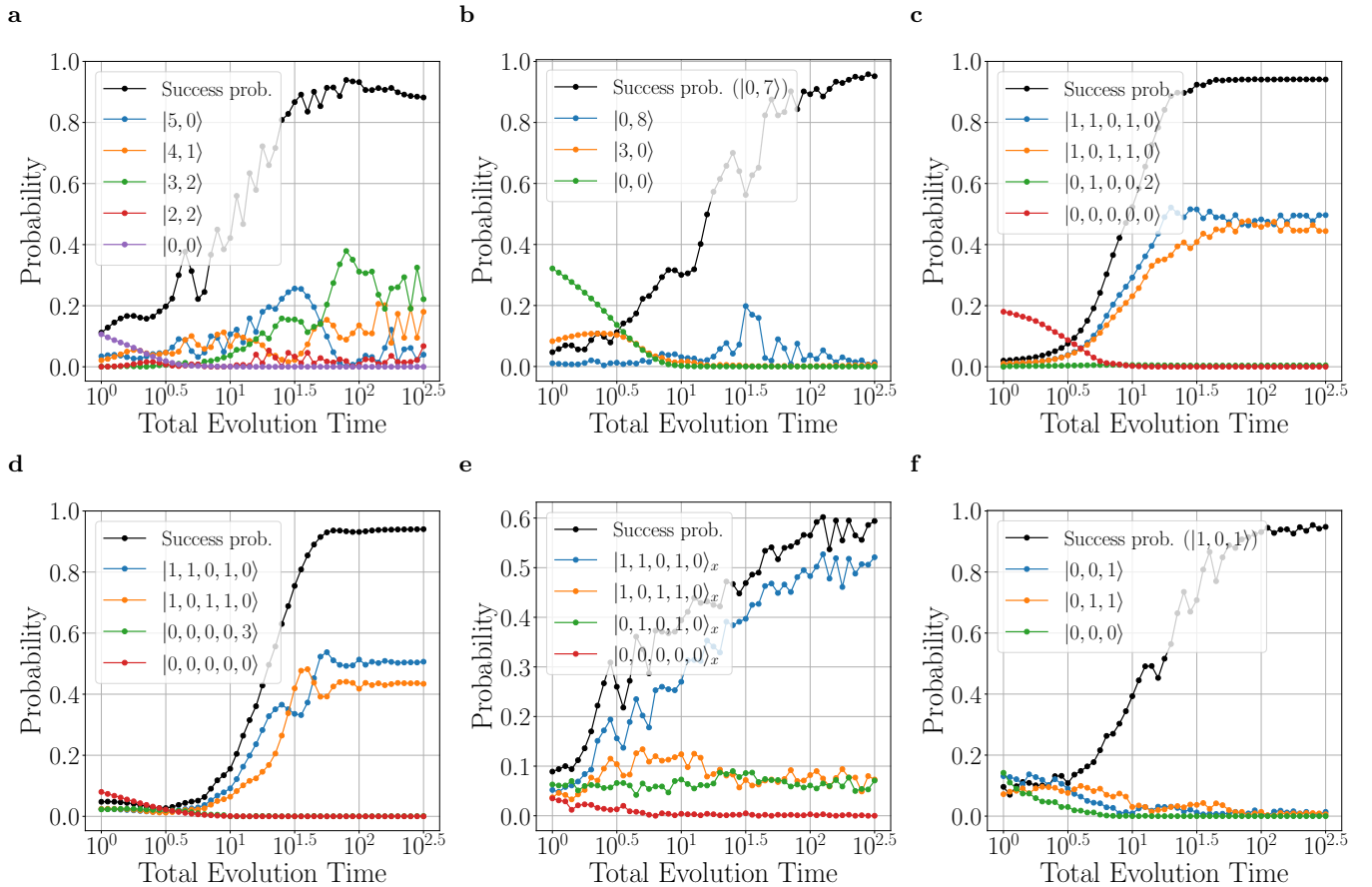


FIG. S1: Adiabaticity plots for the problem types studied: (a) simple integer linear programming (see Section III of the main manuscript); (b) the unbounded knapsack problem (Section III); (c) the binary non-linear integer programming formulation of the MAXCLIQUE problem (Section IV); (d) the integer Motzkin–Straus formulation of the MAXCLIQUE problem (Section V); (e) the continuous Motzkin–Straus formulation of the MAXCLIQUE problem (Section V); and (f) the MIP sparse optimization problem (Section VI). The plots show the evolution of the success probabilities of solving the problems, as well as the probabilities of finding suboptimal solutions, for different values of the total evolution time T . Note that here, for each value of T , each data point represents the probabilities at the end of an individual adiabatic evolution process, whereas in Fig. 1 to Fig. 5 of the main manuscript, each plot represents a single evolution. Other than the parameter T , the parameters used for these simulations are the same as those used in Fig. 1 to Fig. 5.

sampling in the MAXCLIQUE problem is attained when both maximum cliques $\{1, 2, 4\}$ and $\{1, 3, 4\}$ are found with equal probabilities by the solver.

Figure S2 shows the fair sampling in the solutions of the integer linear programming (ILP) and MAXCLIQUE problems discussed in the main manuscript. The plots show the biases of the probabilities of finding the solutions as a function of the value of p_0 defining the mixing Hamiltonian Eq. (3). All of the qumodes are initialized as the squeezed coherent states $|\alpha, -\mathbf{r}\rangle$, where $\alpha = (\alpha_1, \alpha_2, \dots, \alpha_N)$, with $\alpha_j = ip_0/\sqrt{2}$ for all j . Having six degenerate solutions, the bias in the solutions of the ILP feasibility problem $n_1 + n_2 = 5$ is described by the standard deviation of the final probabilities of the solution states $|0, 5\rangle$, $|1, 4\rangle$, $|2, 3\rangle$, $|3, 2\rangle$, $|4, 1\rangle$, and $|5, 0\rangle$. A zero value for the standard deviation means that all six states have equal final probabilities. Figure S2a shows the standard deviation of the probabilities of the six solution states (shown using a purple curve), as well as the probabilities of the three states $|0, 5\rangle$, $|1, 4\rangle$, and $|2, 3\rangle$, the success probability (the sum of the probabilities of these six states), and the total probability (black curve). Due to the symmetry of the problem between n_1 and n_2 in $|n_1, n_2\rangle$, the probabilities of finding the other three states are the same as those for the states shown, with the boson number observables swapped. Figure S3 shows the probability distributions of the final quantum states in the two-qumode Fock basis $\{|n_1, n_2\rangle\}$, for three different p_0 values. As shown, by changing a single parameter p_0 , one is able to adjust the distribution over the probabilities of the solution states, until a “fair” distribution has been reached. Here, a value of $p_0/\sqrt{\hbar} = 0.72$ gives the most even probability distribution among all solution quantum states for the studied ILP feasibility problem. This is also evident from the minimum of the standard deviation of these probabilities at $p_0/\sqrt{\hbar} = 0.72$ in Fig. S2a.

Figure S2b and Fig. S2c show the results of our fair sampling analysis for the MAXCLIQUE problem using formulations (8) and (12). The bias value is defined as $b = \frac{P_{s1} - P_{s2}}{P_{s1} + P_{s2}}$, where P_{s1} and P_{s2} are the final probabilities of finding the two degenerate solutions $\{1, 2, 4\}$ and $\{1, 3, 4\}$, respectively. As shown using a purple curve in Fig. S2b and S2c, a bias of zero means that the two solutions have equal final probabilities.

S3. PARAMETERS IN THE MOTZKIN–STRAUS FORMALISM OF THE MAXCLIQUE PROBLEM

As mentioned earlier, for the integer representation of the Motzkin–Straus formalism (12), the parameter σ is set equal to the size ξ of the maximum clique(s) to find a solution with high probability. As this value is not a priori known, a binary search can be performed to find its value by solving $\mathcal{O}(\log(|V|))$ instances of problem (12) using different choices of $\sigma \in \{1, \dots, |V|\}$. In this section, we study the case when the parameter σ is larger than the size of the maximum clique of the problem and show that even though optimization problem (12) may no longer be equivalent to problem (10), the correct results can still be inferred.

Figure S4 shows the success probability, as well as the probability of finding either of the two solutions, as a function of the hyperparameter λ for the MAXCLIQUE problem shown in Fig. 3a. The probability of finding a

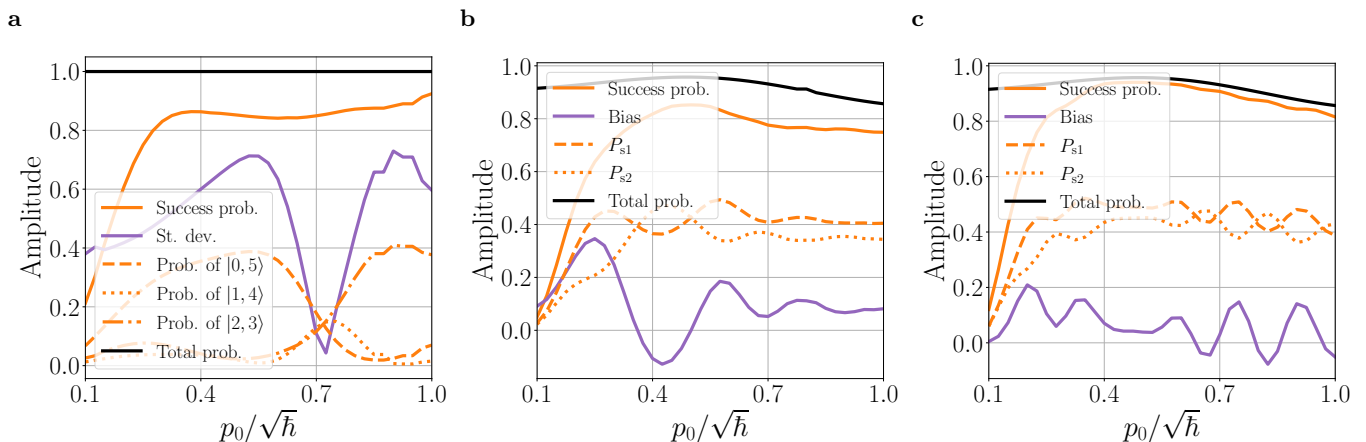


FIG. S2: Fair sampling results for the integer linear programming feasibility problem, and for the two non-integer linear programming formulations of the MAXCLIQUE problem. The success probabilities, and standard deviation or bias of the probabilities of the solution states, as a function of p_0 , are shown using a solid orange and solid purple curve, respectively. All qumodes are initialized with $p_{0i} = p_0$. The bias for the integer linear programming problem is evaluated by finding the standard deviation of the probabilities of the solution states. The bias in panels (b) and (c) for the MAXCLIQUE problem is defined as $b = \frac{P_{s1} - P_{s2}}{P_{s1} + P_{s2}}$, where P_{s1} and P_{s2} are the success probabilities for the two degenerate solutions of the studied problem. Other than the p_{0i} values, the parameters used for these simulations are the same as those used in Fig. 1, Fig. 3b, and Fig. 4b. The total probability (black curves) is obtained as the sum of probabilities of all quantum states within the truncated Fock space (resulting in a total probability value smaller than 1).

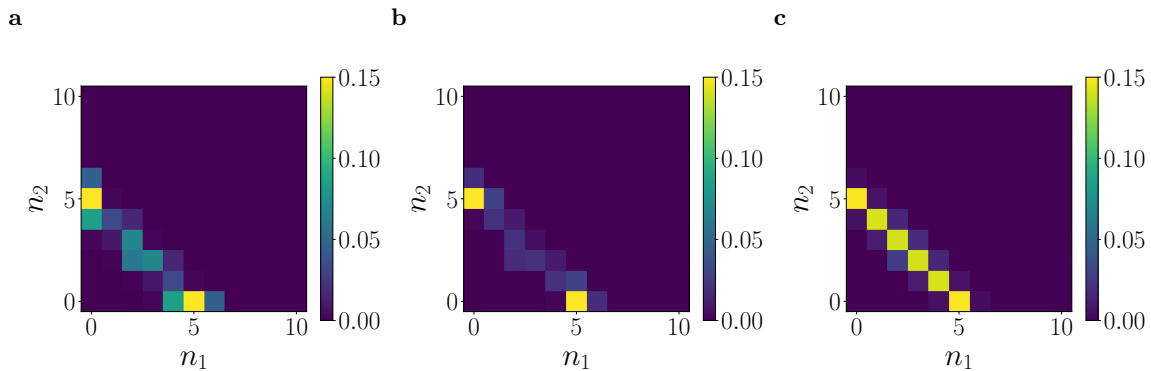


FIG. S3: Dependence of the probability distribution of the final quantum states, in the two-qumode Fock basis $\{|n_1, n_2\rangle\}$, on the parameter p_0 for the feasibility problem specified by the equation $n_1 + n_2 = 5$. The plots are for (a) $p_0/\sqrt{\hbar} = 0.2$, (b) $p_0/\sqrt{\hbar} = 0.5$, and (c) $p_0/\sqrt{\hbar} = 0.72$. Note that the value $p_0/\sqrt{\hbar} = 0.72$ corresponds to the most “fair” sampling of the six solution quantum states. This is also evident in Fig. S2a, from the minimum of the standard deviation of the probabilities of the solution Fock states (shown using a purple curve), at $p_0/\sqrt{\hbar} = 0.72$.

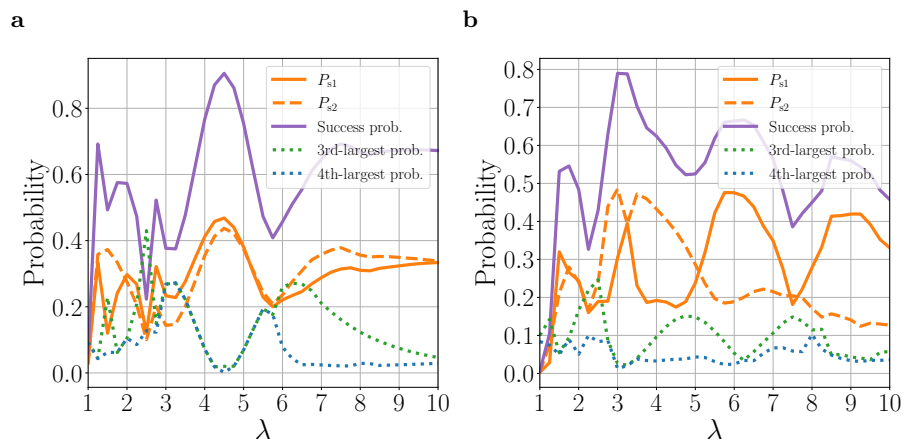


FIG. S4: Success probability of solving optimization problem (12) without knowing the maximum clique size ξ . Shown is the probability of finding the solutions P_{s1} and P_{s2} (defined in Eqs. (S1)), as well as the success probability $P_s = P_{s1} + P_{s2}$, when $\sigma > \xi$, as a function of the hyperparameter λ in the problem Hamiltonian (13). The results are for (a) $\sigma = 4$ and (b) $\sigma = 5$ for the problem shown in Fig. 3a, for which the maximum clique size is $\xi = 3$. As shown in these plots, by tuning λ , one is still able to find the solutions to the MAXCLIQUE problem.

particular solution here is defined as the sum of the probabilities of all of the states that have one or more photons in the qumodes corresponding to the maximum clique. For the maximum cliques given by the vertices $\{1, 2, 4\}$ and $\{1, 3, 4\}$, the solution probabilities are given by

$$P_{s1} = \sum_{n_1, n_2, n_4=1}^d \langle n_1, n_2, 0, n_4, 0 | \psi \rangle \quad \text{and} \quad P_{s2} = \sum_{n_1, n_3, n_4=1}^d \langle n_1, 0, n_3, n_4, 0 | \psi \rangle, \quad (\text{S1})$$

respectively, where $|\psi\rangle$ is the final quantum state prepared using AQC. Here, d is the truncation dimension of the Fock space, which is physically infinite but in a classical simulation must be finite. As shown in Fig. S4, there is an optimal choice of λ at which the largest success probability for a given value of σ is reached. This method of finding the success probabilities aligns well with the functionality of single-photon avalanche detectors (SPAD), where the arrival of one or more photons is detected without the capability to resolve the photon number. The results in Fig. S4 indicate that the maximum cliques correspond to the qumodes that have nonzero photon numbers and thus can be measured using currently available SPADs.

-
- [1] M. W. Johnson, M. H. Amin, S. Gildert, T. Lanting, F. Hamze, N. Dickson, R. Harris, A. J. Berkley, J. Johansson, P. Bunyk, *et al.*, Quantum annealing with manufactured spins, *Nature* **473**, 194 (2011).
- [2] A. Montanaro, Quantum speedup of branch-and-bound algorithms, *Physical Review Research* **2**, 013056 (2020).
- [3] J. Van Apeldoorn, A. Gilyén, S. Gribling, and R. de Wolf, Quantum sdp-solvers: Better upper and lower bounds, *Quantum* **4**, 230 (2020).
- [4] C.-M. Alexandru, E. Bridgett-Tomkinson, N. Linden, J. MacManus, A. Montanaro, and H. Morris, Quantum speedups of some general-purpose numerical optimisation algorithms, *Quantum Science and Technology* **5**, 045014 (2020).
- [5] G. Brassard, P. Hoyer, M. Mosca, and A. Tapp, Quantum amplitude amplification and estimation, *Quantum Computation and Quantum Information: A Millennium Volume*. AMS Contemporary Mathematics Series (2000).
- [6] K. Sankar, A. Scherer, S. Kako, S. Reifenstein, N. Ghadermarzy, W. B. Krayenhoff, Y. Inui, E. Ng, T. Onodera, P. Ronagh, *et al.*, Benchmark study of quantum algorithms for combinatorial optimization: Unitary versus dissipative, arXiv preprint arXiv:2105.03528 (2021).
- [7] S. Lloyd and S. L. Braunstein, Quantum computation over continuous variables, *Phys. Rev. Lett.* **82**, 1784 (1999).
- [8] J. B. Spring, B. J. Metcalf, P. C. Humphreys, W. S. Kolthammer, X.-M. Jin, M. Barbieri, A. Datta, N. Thomas-Peter, N. K. Langford, D. Kundys, J. C. Gates, B. J. Smith, P. G. R. Smith, and I. A. Walmsley, Boson sampling on a photonic chip, *Science* **339**, 798 (2013).
- [9] M. Tillmann, B. Dakić, R. Heilmann, S. Nolte, A. Szameit, and P. Walther, Experimental boson sampling, *Nature Photonics* **7**, 540 (2013).
- [10] H.-S. Zhong, L.-C. Peng, Y. Li, Y. Hu, W. Li, J. Qin, D. Wu, W. Zhang, H. Li, L. Zhang, Z. Wang, L. You, X. Jiang, L. Li, N.-L. Liu, J. P. Dowling, C.-Y. Lu, and J.-W. Pan, Experimental gaussian boson sampling, *Science Bulletin* **64**, 511 (2019).
- [11] C. Weedbrook, S. Pirandola, R. García-Patrón, N. J. Cerf, T. C. Ralph, J. H. Shapiro, and S. Lloyd, Gaussian quantum information, *Reviews of Modern Physics* **84**, 621 (2012).
- [12] T. R. Bromley, J. M. Arrazola, S. Jahangiri, J. Izaac, N. Quesada, A. D. Gran, M. Schuld, J. Swinarton, Z. Zabaneh, and N. Killoran, Applications of near-term photonic quantum computers: software and algorithms, *Quantum Science and Technology* **5**, 034010 (2020).
- [13] N. C. Menicucci, P. van Loock, M. Gu, C. Weedbrook, T. C. Ralph, and M. A. Nielsen, Universal quantum computation with continuous-variable cluster states, *Phys. Rev. Lett.* **97**, 110501 (2006).
- [14] S. Yokoyama, R. Ukai, S. C. Armstrong, C. Sornphiphatphong, T. Kaji, S. Suzuki, J.-i. Yoshikawa, H. Yonezawa, N. C. Menicucci, and A. Furusawa, Ultra-large-scale continuous-variable cluster states multiplexed in the time domain, *Nature Photonics* **7**, 982 (2013).
- [15] J. Roslund, R. M. de Araújo, S. Jiang, C. Fabre, and N. Treps, Wavelength-multiplexed quantum networks with ultrafast frequency combs, *Nature Photonics* **8**, 109 (2014).
- [16] G. Sierksma and Y. Zwols, *Linear and integer optimization: theory and practice* (CRC Press, 2015).
- [17] R. M. Karp, Reducibility among combinatorial problems, in *Complexity of computer computations* (Springer, 1972) pp. 85–103.
- [18] C. A. Floudas, *Nonlinear and mixed-integer optimization: fundamentals and applications* (Oxford University Press, 1995).
- [19] D. Li and X. Sun, *Nonlinear integer programming*, Vol. 84 (Springer Science & Business Media, 2006).
- [20] S. Burer and A. N. Letchford, Non-convex mixed-integer nonlinear programming: A survey, *Surveys in Operations Research and Management Science* **17**, 97 (2012).
- [21] P. M. Pardalos and G. Schnitger, Checking local optimality in constrained quadratic programming is np-hard, *Operations Research Letters* **7**, 33 (1988).
- [22] M. Cerezo, A. Arrasmith, R. Babbush, S. C. Benjamin, S. Endo, K. Fujii, J. R. McClean, K. Mitarai, X. Yuan, L. Cincio, *et al.*, Variational quantum algorithms, *Nature Reviews Physics* , 1 (2021).
- [23] G. Verdon, J. M. Arrazola, K. Brádler, and N. Killoran, A quantum approximate optimization algorithm for continuous problems, arXiv preprint arXiv:1902.00409 (2019).
- [24] E. Farhi, J. Goldstone, and S. Gutmann, A quantum approximate optimization algorithm, arXiv preprint arXiv:1411.4028 (2014).
- [25] G. S. Lueker, *Two NP-complete problems in nonnegative integer programming* (Princeton University. Department of Electrical Engineering, 1975).
- [26] T. S. Motzkin and E. G. Straus, Maxima for graphs and a new proof of a theorem of turán, *Canadian Journal of Mathematics* **17**, 533 (1965).
- [27] D. Bienstock, Computational study of a family of mixed-integer quadratic programming problems, *Mathematical programming* **74**, 121 (1996).
- [28] A. M. Tillmann, D. Bienstock, A. Lodi, and A. Schwartz, Cardinality minimization, constraints, and regularization: A survey, arXiv preprint arXiv:2106.09606 (2021).
- [29] J. L. O’Brien, A. Furusawa, and J. Vučković, Photonic quantum technologies, *Nature Photonics* **3**, 687 (2009).
- [30] C. Sparrow, E. Martín-López, N. Maraviglia, A. Neville, C. Harrold, J. Carolan, Y. N. Joglekar, T. Hashimoto, N. Matsuda, J. L. O’Brien, D. P. Tew, and A. Laing, Simulating the vibrational quantum dynamics of molecules using photonics, *Nature* **557**, 660 (2018).

- [31] J. M. Arrazola, V. Bergholm, K. Brádler, T. R. Bromley, M. J. Collins, I. Dhand, A. Fumagalli, T. Gerrits, A. Goussev, L. G. Helt, J. Hundal, T. Isacsson, R. B. Israel, J. Izaac, S. Jahangiri, R. Janik, N. Killoran, S. P. Kumar, J. Lavoie, A. E. Lita, D. H. Mahler, M. Menotti, B. Morrison, S. W. Nam, L. Neuhaus, H. Y. Qi, N. Quesada, A. Repeatingon, K. K. Sabapathy, M. Schuld, D. Su, J. Swinarton, A. Száva, K. Tan, P. Tan, V. D. Vaidya, Z. Vernon, Z. Zabaneh, and Y. Zhang, Quantum circuits with many photons on a programmable nanophotonic chip, *Nature* **591**, 54 (2021).
- [32] T. Rudolph, Why i am optimistic about the silicon-photon route to quantum computing, *APL Photonics* **2**, 030901 (2017).
- [33] N. Killoran, J. Izaac, N. Quesada, V. Bergholm, M. Amy, and C. Weedbrook, Strawberry Fields: A Software Platform for Photonic Quantum Computing, *Quantum* **3**, 129 (2019).
- [34] R. Yanagimoto, T. Onodera, E. Ng, L. G. Wright, P. L. McMahon, and H. Mabuchi, Engineering a kerr-based deterministic cubic phase gate via gaussian operations, *Phys. Rev. Lett.* **124**, 240503 (2020).
- [35] W. R. Clements, P. C. Humphreys, B. J. Metcalf, W. S. Kolthammer, and I. A. Walmsley, Optimal design for universal multiport interferometers, *Optica* **3**, 1460 (2016).
- [36] N. C. Harris, G. R. Steinbrecher, M. Prabhu, Y. Lahini, J. Mower, D. Bunandar, C. Chen, F. N. C. Wong, T. Baehr-Jones, M. Hochberg, S. Lloyd, and D. Englund, Quantum transport simulations in a programmable nanophotonic processor, *Nature Photonics* **11**, 447 (2017).
- [37] J. Wang, S. Paesani, Y. Ding, R. Santagati, P. Skrzypczyk, A. Salavrakos, J. Tura, R. Augusiak, L. Mančinska, D. Bacco, D. Bonneau, J. W. Silverstone, Q. Gong, A. Acín, K. Rottwitt, L. K. Oxenløwe, J. L. O'Brien, A. Laing, and M. G. Thompson, Multidimensional quantum entanglement with large-scale integrated optics, *Science* **360**, 285 (2018).
- [38] I. L. Chuang and Y. Yamamoto, Simple quantum computer, *Phys. Rev. A* **52**, 3489 (1995).
- [39] J. H. Shapiro, Single-photon kerr nonlinearities do not help quantum computation, *Phys. Rev. A* **73**, 062305 (2006).
- [40] J. Gea-Banacloche, Impossibility of large phase shifts via the giant kerr effect with single-photon wave packets, *Phys. Rev. A* **81**, 043823 (2010).
- [41] B. He and A. Scherer, Continuous-mode effects and photon-photon phase gate performance, *Phys. Rev. A* **85**, 033814 (2012).
- [42] I. Fushman, D. Englund, A. Faraon, N. Stoltz, P. Petroff, and J. Vučković, Controlled phase shifts with a single quantum dot, *Science* **320**, 769 (2008).
- [43] D. Tiarks, S. Schmidt-Eberle, T. Stolz, G. Rempe, and S. Dürr, A photon–photon quantum gate based on rydberg interactions, *Nature Physics* **15**, 124 (2019).
- [44] C. Hamsen, K. N. Tolazzi, T. Wilk, and G. Rempe, Strong coupling between photons of two light fields mediated by one atom, *Nature Physics* **14**, 885 (2018).
- [45] S. Sagona-Stophel, R. Shahrokshahi, B. Jordaan, M. Namazi, and E. Figueroa, Conditional π -phase shift of single-photon-level pulses at room temperature, *Phys. Rev. Lett.* **125**, 243601 (2020).
- [46] E. Farhi, J. Goldstone, S. Gutmann, and M. Sipser, Quantum computation by adiabatic evolution, arXiv preprint arXiv: quant-ph/0001106 (2000).
- [47] E. J. Crosson and D. A. Lidar, Prospects for quantum enhancement with diabatic quantum annealing, *Nat. Rev. Phys.* **3**, 466–489 (2021).
- [48] M. Maamache and Y. Saadi, Adiabatic theorem and generalized geometrical phase in the case of continuous spectra, *Phys. Rev. Lett.* **101**, 150407 (2008).
- [49] C. Gerry, P. Knight, and P. L. Knight, *Introductory quantum optics* (Cambridge university press, 2005).
- [50] D. Crawford, A. Levit, N. Ghadermarzy, J. S. Oberoi, and P. Ronagh, Reinforcement learning using quantum boltzmann machines, *Quantum Information and Computation* **18** (2018).
- [51] B. Sepehry, E. Iranmanesh, M. P. Friedlander, and P. Ronagh, Quantum algorithms for structured prediction, arXiv preprint arXiv:1809.04091 (2018).
- [52] I. M. Bomze, M. Budinich, P. M. Pardalos, and M. Pelillo, The maximum clique problem, in *Handbook of Combinatorial Optimization: Supplement Volume A*, edited by D.-Z. Du and P. M. Pardalos (Springer US, Boston, MA, 1999) pp. 1–74.
- [53] M. S. Könz, G. Mazzola, A. J. Ochoa, H. G. Katzgraber, and M. Troyer, Uncertain fate of fair sampling in quantum annealing, *Phys. Rev. A* **100**, 030303 (2019).